Journal of Great Lakes Research 44 (2018) 14–25

Contents lists available at ScienceDirect

Journal of Great Lakes Research

journal homepage: www.elsevier.com/locate/jglr

Evidence from field measurements and satellite imaging of impact of Earth rotation on Lake Iseo chemistry

Marco Pilotti [a], Giulia Valerio [a], Claudia Giardino [b], Mariano Bresciani [b], Steven C. Chapra [c,*]

[a] DICATAM, Università degli Studi di Brescia, Brescia, Italy
[b] National Research Council–Institute for Electromagnetic Sensing of the Environment (CNR-IREA), Via Bassini 15, 20133 Milan, Italy
[c] Civil and Environmental Engineering, Tufts University, Medford, MA, United States

ARTICLE INFO

Article history:
Received 13 June 2017
Accepted 22 October 2017

Communicated by Barry Lesht

Keywords:
Deep lakes
Tributary inflow
Coriolis force
Lake experimental investigation
Remote sensing
Water resources management

ABSTRACT

During an initial field survey in 2012, we observed an unexpected asymmetry of dissolved oxygen distribution between the western and eastern side in northern Lake Iseo. Motivated by this apparent anomaly, we conducted a detailed field investigation, and we used a physical model of the northern part of the lake to understand the influences that might affect the distribution of material in the northern section of the lake. These investigations suggested that the Earth's rotation has significant influence on the inflow of the lake's two main tributaries. In order to further crosscheck the validity of these results, we conducted a careful analysis at a synoptic scale using images acquired during thermally unstratified periods by Landsat-8 and Sentinel-2 satellites. We retrieved and post-processed a large set of images, providing conclusive evidence of the role exerted by the Earth's rotation on pollutant transport in Lake Iseo and of the greater environmental vulnerability of the north-west shore of this lake, where important settlements are located. Our study confirms the necessity for three-dimensional hydrodynamic models including Coriolis effect in order to effectively predict local impacts of inflows on nearshore water quality of medium-sized elongated lakes of similar scale to Lake Iseo.

Introduction

The growing anthropogenic stress exerted on many lakes in the world (e.g., Wetzel, 1992; Özkundakci et al., 2014) motivates concern for their endangered trophic states. In Europe, the Water Framework Directive (European Parliament, 2000) requires that water bodies be returned to a condition as close as possible to their natural status. This ambitious task might be very challenging, particularly for deep lakes that are usually characterised by long water renewal times. In the case of Lake Iseo, a deep Italian prealpine lake, the theoretical renewal time is 4.5 years but its actual value is 60% longer due to the thermal stratification of the lake during most of the year (Pilotti et al., 2014b). The renewal time is expected to increase further due to the effects of climate change (Pilotti et al., 2014b). The lake's trophic reference condition dates back to 1967 (Bonomi and Gerletti, 1967), when two vertical profiles of physical and chemical properties in spring and winter showed that the lake was oligotrophic with oxygen concentrations of about 8 mg/l at the maximum depth of 250 m. In contrast, we recently observed during several field campaigns that the current situation is characterised by hypoxia below 80 m and total anoxia below 110 m. Such a dramatic evolution should stimulate concern. Although several countermeasures to limit nutrient inputs have been introduced and a combined sewer has been operating for the last 15 years along the lake's periphery, the sewage from the lake's large watershed is still partly untreated and the average concentration of phosphorus in the lake is not decreasing. Similar to other cases (e.g., Chen et al., 2004; Chen and Driscoll, 2009; Halder et al., 2013; Chomicki et al., 2016), in Lake Iseo the preponderance of the watershed loading enters from the tributaries with high concentrations of dissolved and particulate matter, nutrients and bacterial pollution during rainy periods when combined sewer weirs overflow into the tributaries. The distribution of these waters in the epilimnetic layer could trigger local algal blooms and exceed maximum permissible pathogen levels for bathing. The spatial distribution of tributary waters is also critical to understanding the current rate of oxygen supply and demand in the intermediate layer between the anoxic bottom and the fully oxygenated surface layer (Fink et al., 2016). Thus, understanding the interplay of the lake's hydrodynamics with the inflows is critical to predicting water quality impacts on this system.

In order to explore these issues in Lake Iseo, an initial campaign monitoring temperature, oxygen concentration, conductivity, turbidity and chlorophyll-a (Chl-a) was conducted in 2012. A more detailed monitoring campaign was replicated in the summer 2014. This latter survey, which collected data at 179 sites, focused on the northern part of the lake to measure physical parameters in the layer between the surface and the depth of 70 m. The large data set was eventually used to

* Corresponding author.
E-mail address: steven.chapra@tufts.edu (S.C. Chapra).

https://doi.org/10.1016/j.jglr.2017.10.005
0380-1330/

reconstruct the spatial pattern of the measured variables. In order to fully exploit the data's information content and to provide more representative visualization than the usual two-dimensional (2D) horizontal and vertical contoured sections, three-dimensional (3D) surfaces were generated with an interpolation technique based on Inverse Distance Weighting (IDW). This involved pre-processing the data using a vertical expansion in order to effectively deal with the anisotropy between vertical and horizontal directions caused by thermal stratification.

The reconstructed 3D surfaces exhibited a marked east-west asymmetry of the parameters distribution, that must reflect some dynamic physical processes. We advance the hypothesis that a primary role is played by the Earth's rotation, combined with bacterial respiration of organic matter conveyed by river-borne intrusions that exceed the oxygen inputs of river water. The net result is an overall negative impact on metalimnetic and hypolimnetic oxygen concentrations (e.g., Chapra, 1997; Bouffard and Perga, 2016). Two mechanisms support this hypothesis. First, during the thermally stratified period, the westward deflection of the two main tributaries flow could be affected by shoretrapped internal Kelvin waves moving cyclonically around the lake (Valerio et al., 2012). Whereas the effect of internal Kelvin waves in very large lakes is restricted to the area adjacent to the shore (Mortimer, 2006, documented a fall to about 2% at a distance of four internal Rossby radii in Lake Michigan, defined as the ratio between the non-rotating phase speed to the inertial frequency), in Lake Iseo Kelvin waves must occupy the whole basin. However, the effectiveness of this mechanism should be hindered by the fact that the orbits of the water particles involved in internal Kelvin waves in deep waters should be closed, so that the net drift in the direction of phase propagation would be negligible. Moreover, when wind is weak or when the lake is thermally unstratified, (i.e., from December to April), internal wave forcing is absent.

The second mechanism that can be invoked is the action of the Earth's rotation on the plume of the entering tributaries (e.g. Griffiths, 1986), which acts permanently to deflect the inflow when the plume's inertia is small compared with the Coriolis force. The relevance of Coriolis force on the river-induced circulation has been shown for large lakes through physical models by, *inter alia*, Rumer and Robson (1968) in Lake Erie, by Li et al. (1975) and Atkinson et al. (1994) in Lake Ontario and by Stewart (1988) in Lake Constance. The effects of Coriolis force were also documented in medium size lakes by Hamblin and Carmack (1978) in Kamloops Lake, and by Morillo et al. (2008) in Coeur d'Alene Lake. In addition, it is mentioned by Laborde et al. (2010) in Lake Como, whose width is comparable to that of lake Iseo and where the river is deflected towards its right-hand shoreline irrespective of wind conditions. The correspondence between sedimentological units in lakes and Coriolis-related currents has been observed in the past by several authors (e.g., Wright and Nydegger, 1980; Hamblin and Carmack, 1978; Hakanson and Janson, 1983) and is also related to the deposition of river-borne pollutants (Hakanson, 1974). This hypothesis was supported by the results of a physical model in Froude and Rossby similarity (Pilotti et al., 2014a), that, however, explored a limited range of Reynolds numbers and did not take into account the direct action of wind forcing. Although an alternating daily wind regime is usually present on this lake (Pilotti et al., 2013), we decided to focus on the permanent effect of the Earth's rotation, that, in thermally stratified periods, is superimposed on the wind-generated internal waves (see also Pilotti et al., 2014a).

The use of satellite images in the current study provided additional insight into the inflow's dynamics. Satellite remote sensing has been often used in limnology (e.g., Lathrop et al., 1990; Chipman et al., 2004; Li et al., 2008; Zhang et al., 2016) and here is used along with images provided by a land-based webcam. We monitored the influence area of the tributaries by enhancing the signal related to turbidity (e.g., Vanhellemont and Ruddick, 2014), according to the algorithm suggested by Brando et al. (2015) operating with Landsat-8 OLI (Operationl Land Imager) data. This sensor provided a synoptic view of the study area with a pixel size of 30 m, that is adequate for observing local to regional scale processes. To visualize turbidity patterns at finer spatial resolution, higher spatial resolution images acquired from fixed webcam and Sentinel-2 data were also used. In particular, the 10 m spatial resolution of Sentinel-2 data is particularly useful for investigating the fine scale patterns of optical properties in inland waters (Toming et al., 2016). Our research clearly indicates that, for the purpose of this type of analysis, the observation period should be selected on the basis of the buoyancy of the inflowing waters with respect to the lake. If interflow is prevailing in a thermally stratified period (summer), remote observations do not provide useful evidence due to the intrusion of the tributary waters under the lake surface. On the other hand, images acquired during the thermally unstratified period highlight systematic evidence of a westward drift of the tributary waters, that, in turn, provides a confirmation of the greater vulnerability of the west coast of the lake with respect to the tributary pollutant loads.

Field site description

Although Lake Iseo has been monitored regularly since the end of the 1970s, previous sampling was primarily conducted at the deepest point along the lake axis just to the west of the large island, Monte Isola (Fig. 1). In the past, specific campaigns did not focus on the northern part of the lake or to study the actual spatial variability of water-quality parameters. In the following, we detail a set of techniques that we used to assess the role exerted by the Coriolis force on the distribution of waters entering from the two major tributaries at the north end of the lake.

Lake Iseo is located in the prealpine area of the Lombardy region (Fig. 1), has a maximum depth of about 256 m, an area of 61 km^2 and a volume of about 8 billion m^3 making it the fifth largest Italian lake in terms of volume. The lake drains a large watershed (1807 km^2) which is about 30 times larger than the lake surface area) and is also one of the most industrialised districts in the Italian Alps. The complex lake hydrodynamics have been previously studied by Valerio et al. (2012), Pilotti et al. (2014a, 2014b) and Hogg et al. (2013).

The Oglio river (inflow at point I1 in Fig. 1) and Canale Italsider (inflow at point I2 in Fig. 1), are the two main tributaries. They are partly fed by the largest Italian glacier (Adamello, 3554 m a.s.l.) and their overall average annual inflow is 55 m^3/s. Approximately 19 km before entering the lake (point J1 in Fig. 1), up to 40 m^3/s (and on average about 29 m^3/s) of Oglio waters are diverted to Canale Italsider and conveyed to a hydropower plant before being returned to the lake at I2. Accordingly, considering that the average value of the overall Oglio discharge which would be exceeded 347 days a year (Q_{347}) is 20.4 m^3/s, it is clear that during most of the year the discharge in the Oglio river downstream of the diversion J1 is limited to the ecological flow.

At the lake's inlet, waters conveyed by Canale Italsider are on average 2 °C colder than those conveyed by the Oglio river (see Fig. 2) and during the summer this difference can rise to 5 °C. Moreover, as shown in Fig. 2, the temperature of these two inflows is usually colder than the temperature of the lake surface but warmer than the lake hypolimnetic water (currently 6.6 °C below 220 m of depth). Accordingly, interflow is the dominant hydrodynamic condition of both these tributaries although during the end of winter they may occasionally flow on the lake surface.

A waste water treatment plant (WWTP) is located along the Oglio river (see symbol in Fig. 1), 900 m upstream of its inlet into Lake Iseo. During rainy periods, due to sewer hydraulic overcharge of the combined sewer, sewage is frequently delivered untreated to the river. In addition, about 30% of the sewage in Valle Camonica, the largest watershed (Fig. 1) is still discharged totally untreated, or only partly processed, into the river. Accordingly, the bacterial and nutrient pollution carried by the Oglio river is, at least occasionally, non negligible.

Two important historical settlements, Lovere and Pisogne (see Fig. 1), are located along the northern part of the study area. The city

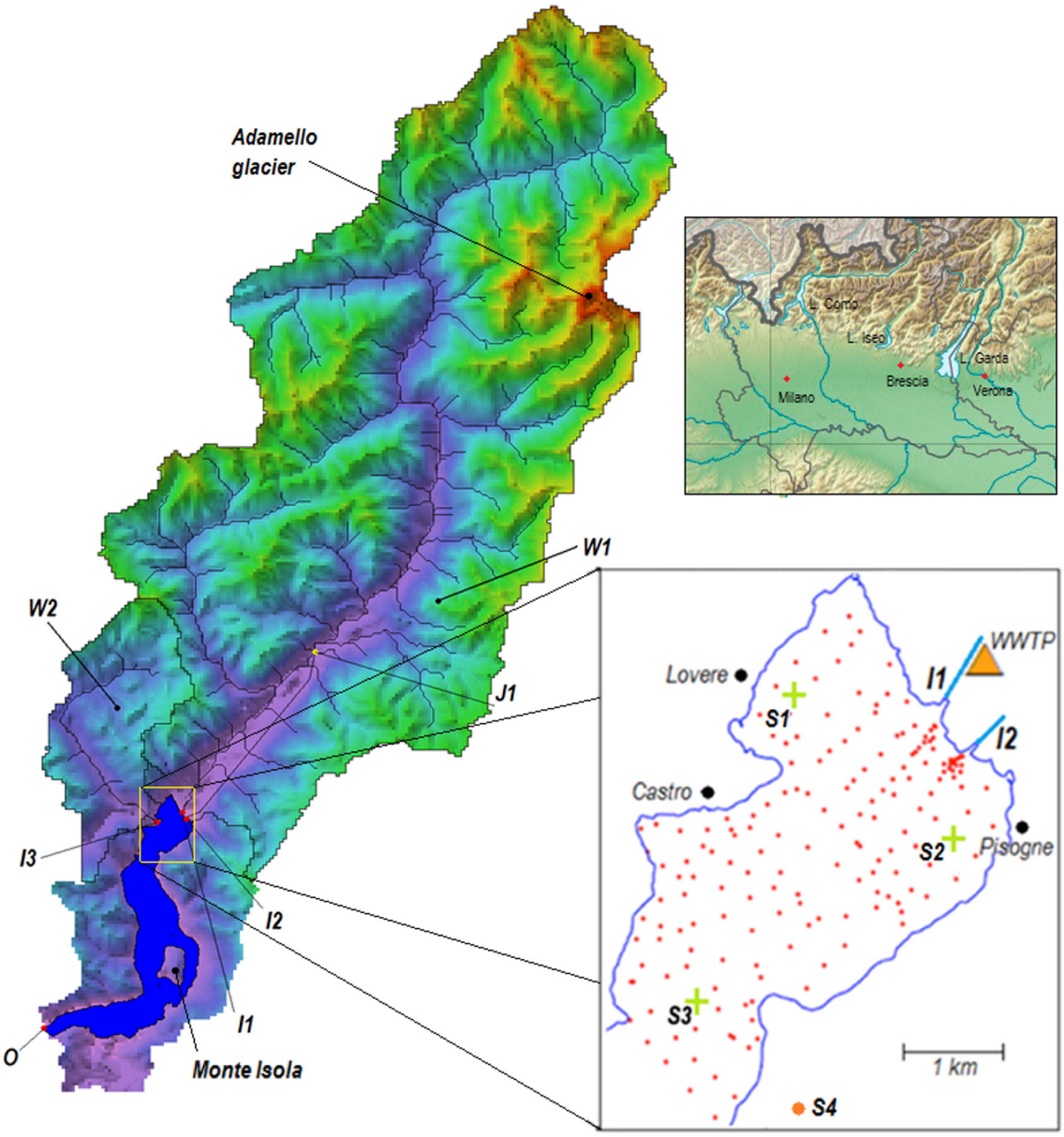

Fig. 1. Lake Iseo within the framework of the Italian prealpine area and of its watershed (overall area of 1807 km^2 at the outlet O). The most relevant sub-catchments are Valle Camonica (W1, 1439 km^2) and Borlezza (W2, 131 km^2). The main natural tributary is Oglio river (inlet at I1), whose waters are partly supplied by the Adamello glacier (3554 m a.s.l.). At point J1 an average discharge of 29 m^3/s is diverted to an artificial canal (Canale Italsider) that conveys water to an hydropower plant, that discharges into the lake at point I2. The inset on the right shows the study area and the locations of the 179 profiles measured in September 2014. WWTP is a large waste water treatment plant located along the Oglio River. S1 and S2 are the locations of the profiles shown in Fig. 3. S3 is the site of a lake diagnostic station where meteorological data are measured in real time and where the profiles shown in Figs. 5 and 12 were taken. Finally, S4 is the position of the webcam used for Fig. 11B.

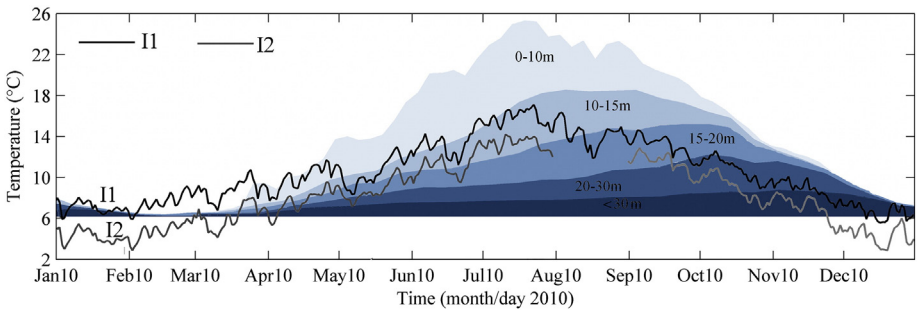

Fig. 2. Yearly temperature stratification of the lake, compared with the measured temperature of the two main tributaries I1 and I2 (data for year 2010).

of Lovere, one of the most touristically important municipalities of the lake, is located in the gulf along the north-west coast. Pisogne is located just to the east of the Canale Italsider.

Methods

Experimental campaign and the 3D data reconstruction

During the first campaign in July 2012, spatial variability of the metalimnetic oxygen distribution below 25 m on the west and east side of the lake was observed. The average oxygen concentration between 20 and 40 m on the western side was up to 1.5 mg/l lower than on the eastern side. In order to better understand the reason for this variability, on 29 and 30 September 2014, an extensive experimental campaign was conducted in the northern part of Lake Iseo, within the area shown in Fig. 1.

Overall, 179 vertical profiles of temperature, conductivity, dissolved oxygen (DO), Chl-a and turbidity were measured between 1 and 70 m, with an average horizontal separation of about 350 m and a vertical resolution of 0.2 m. This vertical resolution was selected on the basis of the computed plunge velocity of the profiler (a RINKO CTD profiler with optical fast DO sensor by JFL Advantech *Co*. Ltd.) and of the short response time of its sensors. The DO sensor was calibrated each morning with two-point measurements, using fully oxygen saturated and desaturated water. Fig. 3 shows a typical vertical profile of the measured variables.

Although 2014 was an exceptionally wet year, the incoming discharge during September 2014 was always below 90 m^3/s, so that the northern part of the lake was not perturbed by recent flood waters. In the 10 days prior to the experimental period, the two main inflows conveyed an overall discharge slowly decreasing from 80 to 50 m^3/s. Temperature and conductivity of the two tributaries were also monitored during the field campaign (see Fig. 4), using two probes located 50 and 200 m upstream of their lake inlets. By comparing these data with the lake temperature profile, we estimated that the depth of intrusion of the two inflows was about 15 m.

The measured data set was used to reconstruct the spatial distribution of the variables. Although many papers have compared different interpolation techniques in a 2D space (e.g., Zimmerman et al., 1999; Li and Heap, 2011; Li et al., 2010, 2011), relatively few papers have addressed the topic of 3D interpolation in stratified water bodies. Murphy et al. (2010), interpolated water quality parameters in the Chesapeake Bay with two different techniques, using a 2D interpolation on layers with thickness from 1 to 2 m. More recently, Sahlin et al. (2014) examined and validated the performance of 2 different 3D spatial interpolation techniques for the marine pelagic environment and concluded that interpolation techniques in a 2D space inevitably cause a loss of spatial information with respect to the complexity of the prototypical 3D processes.

Interpolation methods provide the estimated value of the variable $\hat{u}(\mathbf{x})$at point $\mathbf{x}$ in space as a weighted average of the n observed values of the variable w_i according to the equation:

$$\hat{u}(\mathbf{x}) = \sum_{i=1}^{n} w_i(\mathbf{x})\, u_i \tag{1}$$

where w_i is the weight at location $\mathbf{x}$ with respect to the i^{th} observed value within the specified neighborhood. According to Li and Heap (2011), who conducted a thorough study on 72 different spatial interpolation methods used in environmental science, inverse distance weighting (IDW), ordinary kriging (OK), and ordinary co-kriging (OCK) are the most frequently used methods to compute the weights. Although there is evidence that in several cases kriging is superior, the fundamental assumption that the mean and variance of the data are invariant with translation does not seem warranted in deep prealpine lakes during thermally stratified periods. On the other hand, considering the large number of observation points, in our case one can expect little difference in the performance of more sophisticated approaches. Accordingly, because of its efficiency and ease of implementation within the MATLAB environment used here, we implemented the 3D Inverse Distance Weighting method (IDW), which is commonly adopted in many environmental applications (e.g. Bahner, 2006).

In the case of the IDW the weights are given by:

$$w_i(\mathbf{x}) = \frac{\frac{1}{d_i^e}}{\sum_{j=1}^{n} \frac{1}{d_j^e}} \tag{2}$$

where the power e typically varies in the range 1–3. Accordingly, the influence of distant points decreases as e increases and usually a maximum distance (*radius*) from the target can be detected beyond which data are simply neglected. The method also does not extrapolate values beyond those of the measured data set.

It is relevant to observe that a true 3D interpolation of the measured parameters in a thermally stratified lake is distorted by the strong anisotropy between vertical and horizontal directions. This anisotropy is

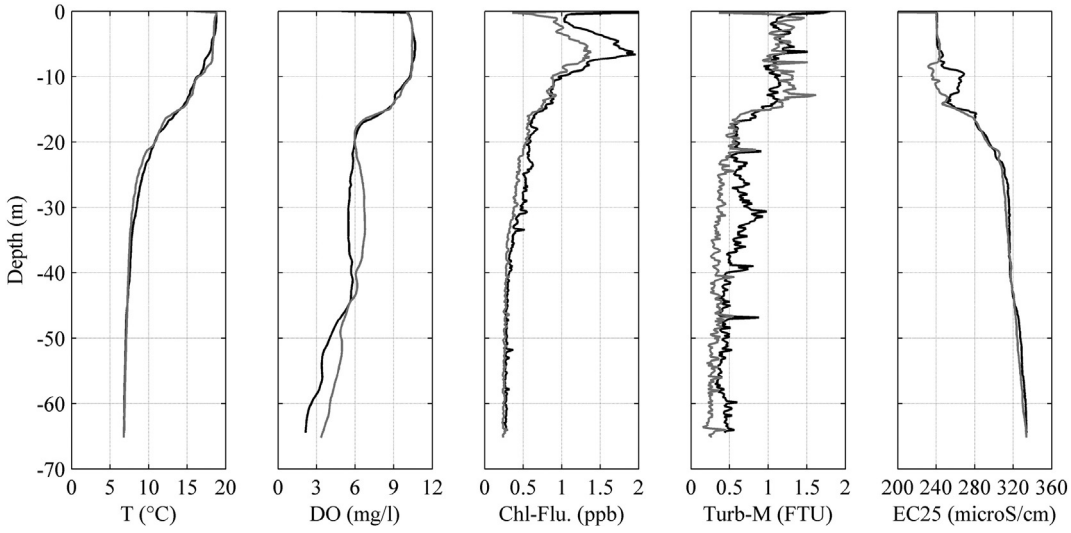

Fig. 3. Contemporaneous profiles of the investigated variables between 0 and 70 m measured at station S1 in the western side of the lake (black line) and S2 in the eastern side (gray line) during stratified season. The location of S1 and S2 is shown in Fig. 1.

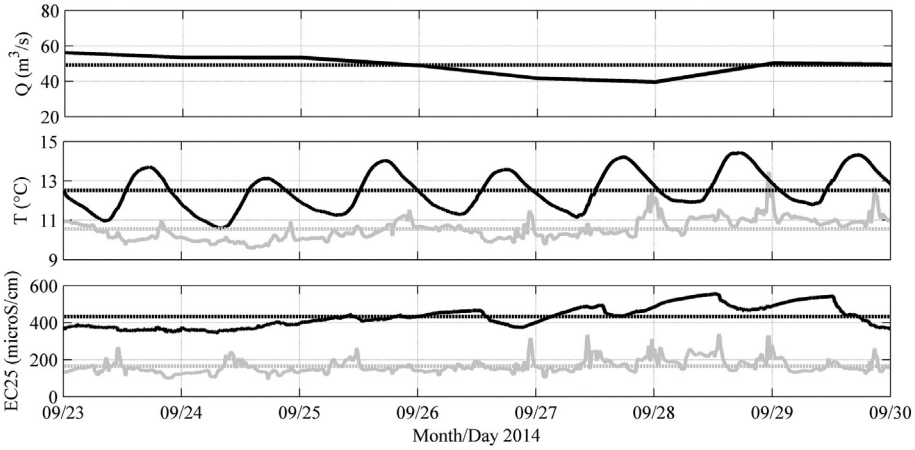

Fig. 4. Overall discharge, temperature and conductivity of the 2 tributaries I1 (black lines) and I2 (gray lines) during the experimental campaign. The dotted lines show the time average for the parameters in the period.

caused by large variations in water stability at the different depths, as shown by typical patterns of the buoyancy frequency. In order to deal with this dilemma we used the approach mentioned by Sahlin et al. (2014), according to which the vertical coordinate z is stretched by a vertical amplification factor α, mapping the data from the xyz space to an xyz̲ grid space, where $\underline{z} = \alpha z$. To this end, for each tentative set of the parameters, a leave-one-out analysis was applied to $n = 179$ measured profiles. In particular, n subset of (n-1) profiles were used to compute the left-out profile and the corresponding overall MRSE between measured and reconstructed data. Whereas Sahlin et al. (2014) used $\alpha = 111$ for the temperature and $\alpha = 800$ for Chl-a concentration, in our case, by minimizing the mean root square error (*MRSE*) between measured and predicted data, the parameters shown in Table 1 were identified for the 3D *IDW* interpolation algorithm. After optimisation of α, the radius, and the exponent, the validation between measured and predicted values (see Fig. 5) is very good. Temperature, normalised conductivity and dissolved oxygen are very well predicted. As far as turbidity and Chl-a are concerned, the fit is less satisfactory, indicating that the characteristic length of the spatial variation of these variables is shorter than the average horizontal distance between the sampling verticals.

The physical model and the supporting evidence from remote sensing

The 2012 campaign suggested that a persistent dynamic process could be the ultimate reason for the observed inhomogeneities. Accordingly, an experimental investigation of the role of Coriolis force was conducted. Although the impact of Coriolis force on the entering waters of a tributary in the case of large lakes is well known (e.g., Atkinson et al., 1994), in medium-sized lakes like Iseo it could be counterbalanced and masked by other important dynamic effects.

A general measure of the significance of rotation is provided by the Rossby number, *Ro*, which is the ratio of the inertial force to the local Coriolis force:

$$Ro = \frac{v}{Lf} \tag{3}$$

Table 1
Optimal set of scaling parameters obtained by minimization of the *MRSE*.

	Conductivity	Chl-a	Turbidity	Oxygen	Temperature
Exponent *e*	1	1	2	1	3
α	**500**	**250**	**150**	**1350**	**650**
Radius [m]	**550**	**450**	**550**	**450**	**1800**
RMSE	**5.024 μS/cm**	**0.075 ppb**	**0.178 FTU**	**0.275 mg/l**	**0.346 °C**

where v and L were selected, respectively, as the average velocity of the interflow (m/s) and a characteristic length scale over which the interflow velocity slows down almost to zero in a typical flow situation (m). $f = 2\omega_P \sin\varphi$ is the Coriolis frequency, where ω_P represents the angular velocity of the Earth (1/s) and φ the latitude (rad). For our case, we measured the average velocity of the interflow $v = 0.04$ m/s using some specifically designed drogues initially deployed in front of the tributary mouth, with the result $Ro \approx 0.13$, which indicates that rotation should be relevant on the prevailing interflow mode that characterises the tributary flow into the lake. In order to test this hypothesis, a rotating vertically distorted physical model of the northern part of this lake was prepared and used, respecting both Froude and Rossby similarity. For a detailed discussion of these experiments see Pilotti et al. (2014a).

In order to simulate the Earth's rotation, the model was mounted on a purposely built revolving table with a diameter of 1.2 m. We explored different hydrologic conditions, by operating both in isothermal and stratified conditions and with different sets of constant inflows from the two tributaries. Although the results of the physical model provide a clear partial explanation of the observed inhomogeneity, this explanation was not regarded as conclusive. Actually, due to the complexity of the prototype situation, a physical model must inevitably introduce a set of simplifying assumptions, so that only partial similarity criteria can be met. For instance, vertical distortion must be inevitably introduced in such a large lake, internal waves cannot be reproduced as well as the effective alternating daily action and distribution of wind (Pilotti et al., 2014a). Finally, the flow Reynolds number is inevitably much lower than the prototypal one, so that Reynolds similarity cannot be fulfilled. Accordingly, one may wonder whether the results are entirely realistic and hence we sought additional confirmation using both satellite and real-time webcam images.

Considering the prevailing interflow mode of the Lake Iseo tributaries, the search for suitable images was directed to the thermally unstratified period between January and April (see Fig. 2). Based on this criterion, a total of six Landsat-8 OLI (Operational Land Imager) cloud-free images were obtined for the period 2013–2016. OLI imagery were radiometrically calibrated according to Pahlevan et al. (2014) and atmospherically corrected with ACOLITE (Atmospheric Correction for OLI 'lite'), an automatic method for OLI atmospheric correction in coastal and inland waters (Vanhellemont and Ruddick, 2014, 2015). The ACOLITE-derived water leaving reflectance were converted to turbidity (T, expressed in formazin turbidity unit - FTU) according to Dogliotti et al. (2015). Although the retrieval of turbidity from Landsat-8 OLI images has a global applicability in a turbidity range of 1–800 FTU (Dogliotti et al., 2015), an evaluation of turbidity retrieval for Lake Iseo was performed. To this end, during the Landsat-8 overpass on 26/09/2016 in situ measurements of suspended particulate matter (SPM, in g/m^3)

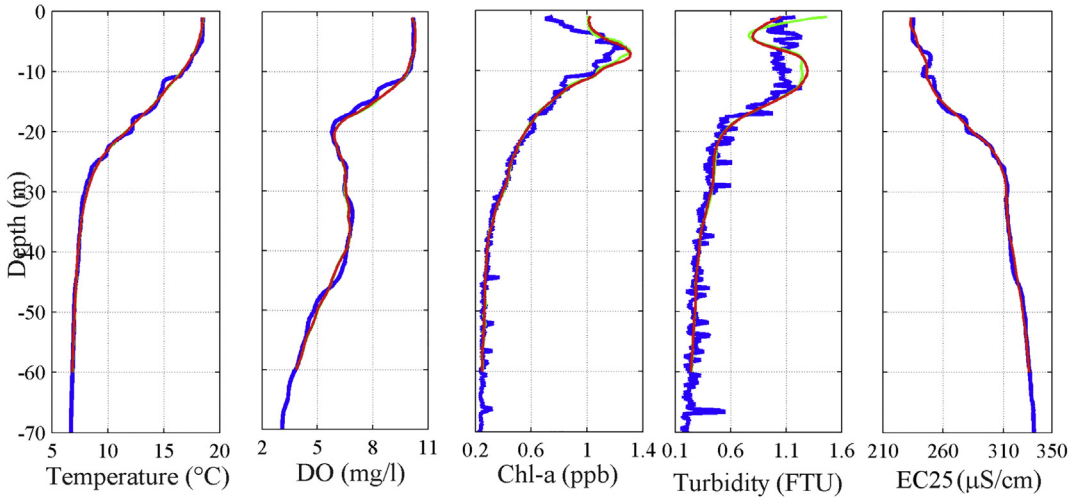

Fig. 5. Example of measured (blue solid line) and predicted with two different algorithms (red and green solid line) profiles at point S3 in Fig. 1. The predicted profiles are computed only on the basis of the data measured at the surrounding sampling profiles and using the optimised vertical expansion.

gathered in five locations were determined gravimetrically (Strömbeck and Pierson, 2001) and compared to satellite derived turbidity. With field measurements ranging from 1.44 g/m^3 to 2.00 g/m^3 (average 1.76 g/m^3), satellite data from 1.69 FTU to 2.41 FTU (average 2.05 FTU) and the Pearson's correlation coefficient of 0.97, we deduced that accurate estimation of turbidity patterns are retrievable from Landsat-8 data of Lake Iseo.

Since December 2016, a real time remote monitoring was operated through a webcam positioned 1000 m above the lake surface, on a mountain facing the tributary's mouth (see point S4 in Fig. 1 and images are available at http://hydraulics.unibs.it/hydraulics/il-monitoraggio-del-lago-diseo/webcam/). The webcam, which was sampled twice an hour during the daylight hours, was intended to supplement the temporally sparse images acquired by satellites. These images can be used for a better understanding of the fate of entering waters, as well as, coupled with the wind measured at S3 (see Fig. 1), for studying the evolution of mixing process such as those caused by Langmuir circulation.

Results

The volumetric VOXEL (VOlume piXEL, Foley et al., 1990) representation of the interpolated data that can be obtained by 3D algorithms, makes it possible to generate different visualizations of the three-dimensional phenomena and is extremely useful for identifying the spatial and temporal extent of criteria exceedances of water quality parameters, such as the ones suggested by EPA (USEPA and Region III Water Protection Division, 2007). As an example, Fig. 6A shows the planimetric map of interpolated dissolved oxygen, averaged in the layer between 5 and 45 m of depth. The vertical averaging was needed in order to filter the transitory effect of internal waves that could affect the visualization within a narrower range of depth. The difference between the oxygen content on the western and eastern side of the lake is striking, with minimum concentration in the bay in front of Lovere. Interestingly, the patterns of conductivity, Chl-a concentration and turbidity (Fig. 6B, C, D) also exhibit coherent spatial trends, with maximum values in the area of the bay of Lovere.

The same asymmetry in DO is visible in the cross-section in Fig. 7D, located 700 m from the tributary inlets, along the transect depicted in Fig. 7A. At 30 m depth, i.e. below the ordinary depth of intrusion of the tributaries, the east-west difference in oxygen concentration ranges between 2 mg/l and 1 mg/l (see Fig. 8). This asymmetry is not explained by the proximity to the sediments, since the depth of the bottom is very similar on the west and east sides of the lake, as illustrated by the cross section in Fig. 7B, where the yellow shading represents the area covered by the vertical map of Fig. 7C–G. The conductivity transect (Fig. 7E) shows the presence of two intrusions between 10 and 17.5 m on the west side. It is interesting to observe that the anomaly inside the Lovere Bay between about 10 and 15 m depth must correspond to the waters of the Oglio river and the deeper one (about 15 to 17.5 m) to the colder waters of the Canale Italsider. The former intrudes into lower

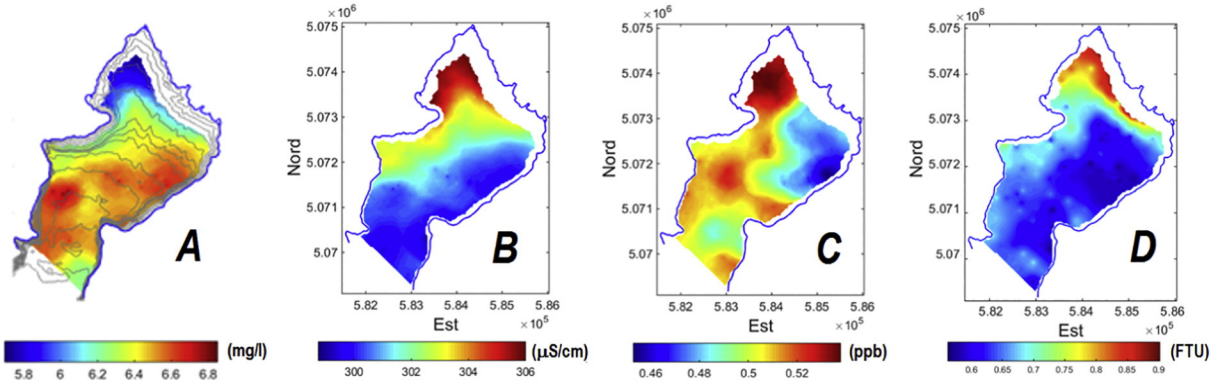

Fig. 6. Average value in the water layer between 5 m and 45 m of depth of (A) oxygen concentration with superimposed bathymetric isodepth lines every 20 m, (B) normalised conductivity at 25 °C, (C) fluorescence signal proportional to Chl-a concentration and (D) turbidity (FTU units).

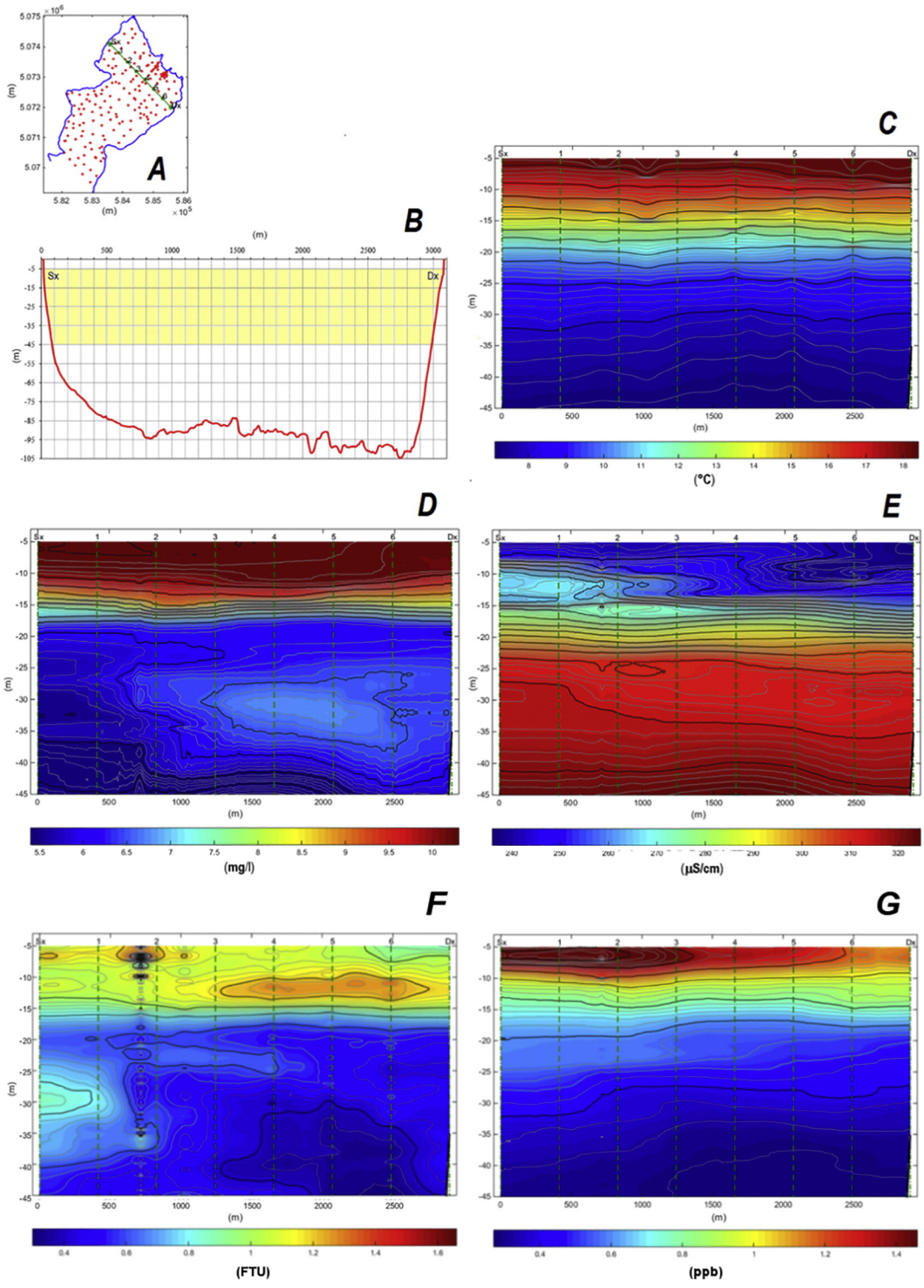

Fig. 7. Vertical cross-sections of temperature (C), dissolved oxygen (D), specific conductivity (E), turbidity (F), and Chl-a concentration (G) along the transect shown planimetrically in (A) and vertically in (B). The shading in cross section (B) corresponds to the area covered by the maps of Fig. C, D, E, F and G.

conductivity epilimnetic waters, so that its presence manifests itself as a positive conductivity anomaly whereas the latter intrudes in the saltier water under the thermocline as a negative anomaly; that is, a lower conductivity than expected. Accordingly, Fig. 7E confirms that the waters of the two tributaries may partly overlap in their westward drift, although at different depths, as also confirmed by the results of the physical model. The dissolved oxygen transect (Fig. 7D) shows a negative concentration anomaly just under the intrusion of the Oglio waters, with respect to surrounding waters at the same depth. It seems resonable to suppose that this corresponds to the metabolic oxygen demand caused by decomposing organic matter that settles from the Oglio waters and, during the thermally stratified period, concentrate above the thermocline, where the buoyancy frequency is at a maximum. On the other hand, a slight positive anomaly is visible corresponding to the Canale Italsider intrusion, whose waters are originally colder and, accordingly, more oxygenated. Finally, also Fig. 7F and G show a clear asymmetry in the east-west distribution of turbidity and Chl-a. In Fig. 7F, the whole mass of water under the thermocline in the western side of the lake is

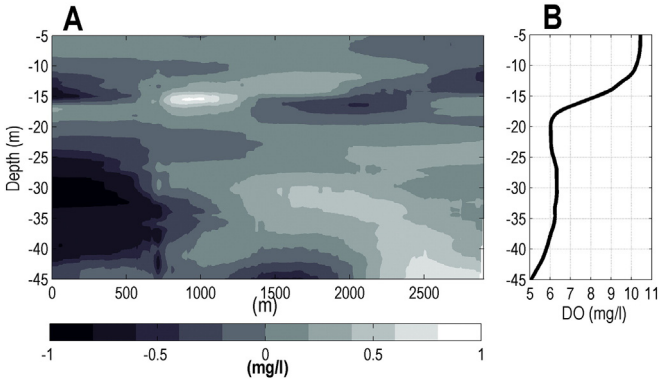

Fig. 8. Difference (A) between the spatial distribution of dissolved oxygen represented in Fig. 7D and the average vertical profile of dissolved oxygen on the same cross section, represented in panel B.

systematically more turbid than the water of the east side. The pattern is not equally clear in the more dynamic mixed layer (0–12 m), where some spots of higher turbidity are present also on the east side. Whereas the spot between cross section 4 and 6 is related to the intruding waters of the industrial canal, the local maximum on the east corner is probably related to a local outfall. The pattern of Chl-a shown in Fig. 7G is characterised by a remarkable maximum in the photic zone on the west side of the lake. The spatial continuity of this maximum indicates the presence of a growing algal population, enhanced by the precence of the nutrient-rich water of the Oglio tributary.

With regard to the oxygen profiles, they usually exhibit a negative heterograde curve which is typically related to a local maximum in dissolved oxygen depletion rates due to microbial and zooplankton respiration, deoxygenated inflowing water, or increased sediment oxygen uptake (Wetzel, 2001). In the top 22 m, all the measured oxygen profiles are similar, indicating a 12-m layer of uniform fully-oxygenated water, followed by a sharp trasition to the metalimentic oxygen minimum lying between 16 and 22 m (see Fig. 3B). In contrast, remarkable spatial differences are present in the underlying layers. In Fig. 3B, we compared profiles taken at two points having the same depth (65 m) but being close to the western and eastern sides of the lake. The western profile has on average 0.9 mg/l less than the eastern one between 20 and 40 m. Interestingly, at the same depths both the Chl-a concentration and turbidity, which are typically used as proxies for oxygen consumption (Kreling et al., 2016), show a maximum closer to the western side. As already observed for the vertical transects, the oxygen pattern could reflect the stronger biochemical oxygen demand of the nutrient rich waters entering from the tributaries, which made the western portion of the lake richer in settling organic matter available for microbial degradation.

The results of the physical model provide a clear dynamic explanation for these observations. Fig. 9A shows the plumes of the Oglio river and Canale Italsider entering Lake Iseo as overflows and conveying an overall discharge of 50 m^3/s (equally split between the two tributaries), which can be regarded as the average yearly inflowing discharge. In general the experiments reproducing plume intrusions do not show a marked difference with respect to those where an overflow occurs, although in the former case the tracer is more confined whereas in the latter there is a stronger lateral dispersion. It is interesting to observe that, as shown in Fig. 9B, if the revolving table is not rotating, the plume axis is rectilinear in front of the tributary mouths. When the Earth's rotation is included, the effect of Coriolis force is clearly noticeable in all the experiments except for the highest discharge. In all the investigated cases there is a clear tendency to curve westward towards the shoreline of Castro peninsula (Fig. 1), forcing a clockwise gyre within the bay of Lovere.

Apparently, in spite of the inevitable simplifications introduced in a laboratory model, this was able to capture the most relevant dynamic forces acting on the inflowing rivers. This is confirmed, at a totally different space scale, by the analysis of satellite images taken at the end of winter when the inflows overflow the lake's water. This observation is not possible during the rest of the year when the typical inflowing mode is an interflow and, accordingly, turbidity gradients do not show up at the surface (see Fig. 13).

Fig. 10 shows the sequence of six Landsat 8-OLI derived maps of turbidity both qualitatively (e.g. extent, shape) and quantitatively (e.g. gradients in FTU with a scale from 0 to 3 FTU). The images depict the turbidity patterns in the period of thermally unstratified waters and the tributary overall discharge and temperature (derived on the basis of a calibrated correlation with local air temperature) in the preceding week, compared with that of the lake surface. In all six images, the turbidity patterns are comparable to the inflow patterns observed observed with the rotating physical model (see Fig. 9A).

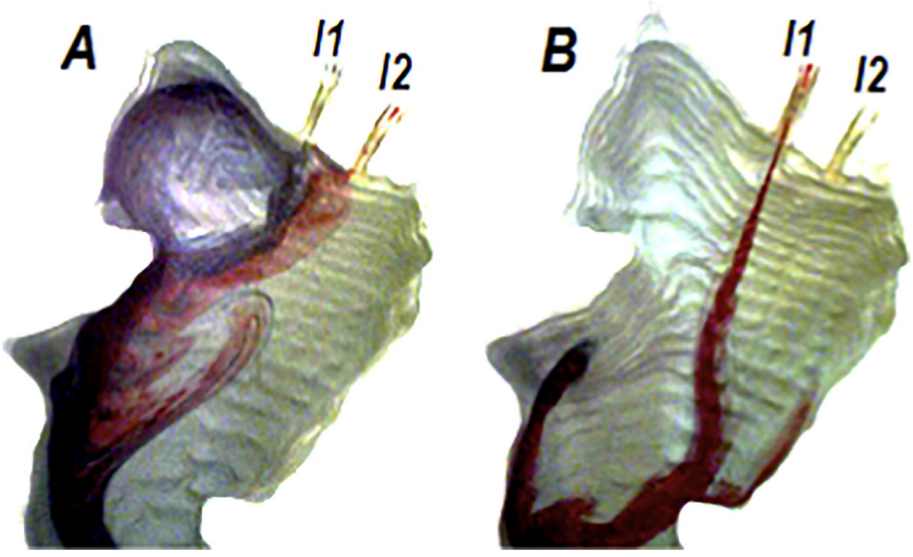

Fig. 9. Visualization of the results of two experiments with the rotating and non-rotating physical model. In case A the lake is thermally unstratified and the tributaries I1 and I2 overflow the lake's water, each conveying the same discharge of 25 m^3/s. In case B the lake is thermally stratified, with I1's temperature 2 °C lower than the lake surface's temperature to simulate an interflow. The discharge from I1 is 50 m^3/s, but the revolving table is not in motion.

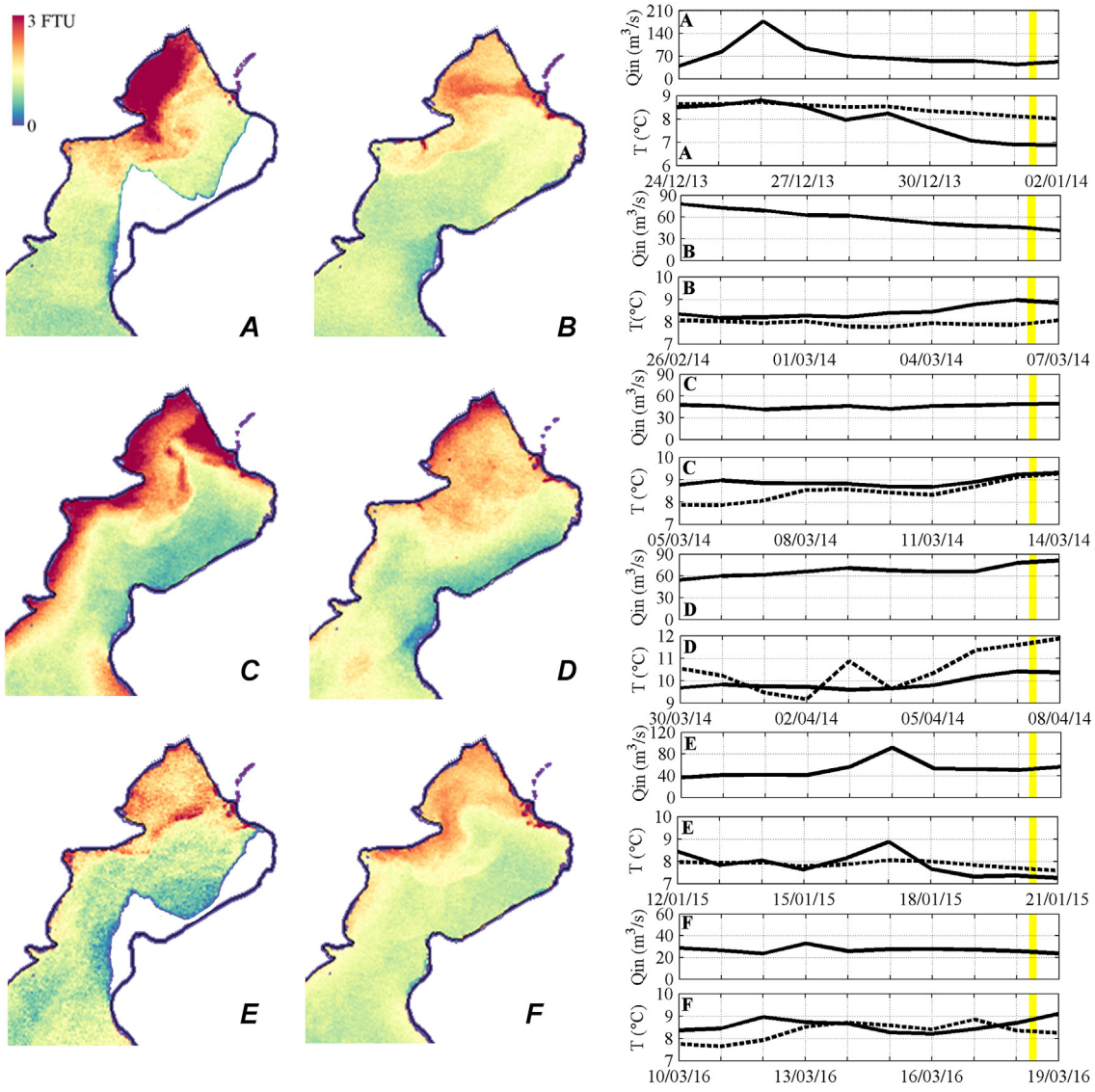

Fig. 10. Landsat-8 maps in the period 1/1/2014–19/3/2016 showing the turbidity (FTU) of surface waters in the northern part of Lake Iseo. In the right panels, the time series of the overall discharge entering the lake, temperature of surface lake (solid line) and the temperature of the I1 tributary (dotted line) are shown with reference to the 8 days before the time of acquisition by the satellite, highlighted by the yellow band. The whitened areas in pictures (A) and (E) correspond to areas sheltered by the shadow of the surrounding mountains.

An exceptional validation of the experimental results shown in Fig. 9A is finally provided by the image taken by the recent Sentinel-2 satellite at 11 AM on 17/2/2017. In this period the power house along the Canale Italsider operated only intermittently from 10 AM to 12 AM with a discharge of 15.2 m^3/s and the average discharge from the Oglio river was 10.8 m^3/s. At the same time, the operation of hydraulic works along the Oglio river upstream of the diversion J1 in Fig. 1, supplied suspended sediment that acted as a natural tracer of the entering waters. During this period the webcam positioned at point S4 in Fig. 1 provided almost simultaneous evidence (see Fig. 11A) of the turbidity plume behavior from two different perspectives during a period of relatively low flow.

Discussion and concluding remarks

Although different forcings (e.g., daily alternating anabatic and katabatic winds) act on the lake, the analysis following the monitoring campaign of September 2014 provided clear evidence of the persistent role of Coriolis force on the fate of tributary waters on the northern part of Lake Iseo. Over the long term, this forcing manifests itself in a different average distribution of physical and chemical properties of the waters between the west and east side of this lake. The evidence was provided through a set of tools and processing operations that enhanced the informative content of the original raw data. Accordingly, the roadmap followed in this paper provides hints that can be useful and that can be replicated at other sites.

As a first step, the information obtained from the 2014 monitoring campaign was interpolated with a 3D *IDW* algorithm, in order to reconstruct their space evolution. The pre-processing of measured data relaxes their original anisotropy by a vertical expansion. After this operation, *IDW* proved to be simple to implement within the MATLAB environment and computationally efficient. It might be interesting to see how the *IDW* algorithm (or any other 3D interpolating algorithm that does not use a variable spatial correlation) would work without the vertical expansion of the data. To this purpose, Fig. 12 provides an example of the profiles predicted at point S3 in Fig. 1, by using the data from the surrounding sampling profiles. Both *IDW* and a *Natural Neighbours* method have been used. The reason for their poor predictive capability compared with optimised vertical expansion (Fig. 5) lies in the anisotropy between horizontal and vertical directions. Moreover,

Fig. 11. RGB images from Sentinel-2 (A) and webcam (B) taken during thermally unstratified period at 11 AM on 16/2/2017. The position of the webcam is shown as S4 in Fig. 1. The overall daily-averaged discharge entering the lake from I1 and I2 tributaries was 25 m^3/s; at 11 AM the hourly-averaged contribution from I1 was 10.8 m^3/s, while the one from I2 was 15.2 m^3/s.

in the presence of layers with different density gradients, vertical correlation varies with depth.

As usual in this type of measurement, the considered data set is very densely distributed along the vertical (data were measured every 20 cm) but sparse in the horizontal (average distance between profiles was on the order of 300 m). Whenever data are spatially interpolated, an influence radius must be introduced under the assumption that correlation between measured values and the predicted one is negatively correlated with distance. If this radius is too small, the information is poorly exploited because the neighborhood of the predicted point could be almost empty. Accordingly, the radius should be scaled on the average distance between the measured profiles. However, this average distance is typically larger than the maximum depth and definitely larger than the length scale provided by the thermocline thickness in a thermally stratified lake, where the suppression of vertical turbulence creates a strong horizontal correlation along the same isopotential surface. Accordingly, by using a 3D interpolation approach, the value of a variable interpolated at a given depth in the neighborhood of a measured profile would be affected by the data measured along the vertical profile, almost irrespective of depth. For instance, the predicted

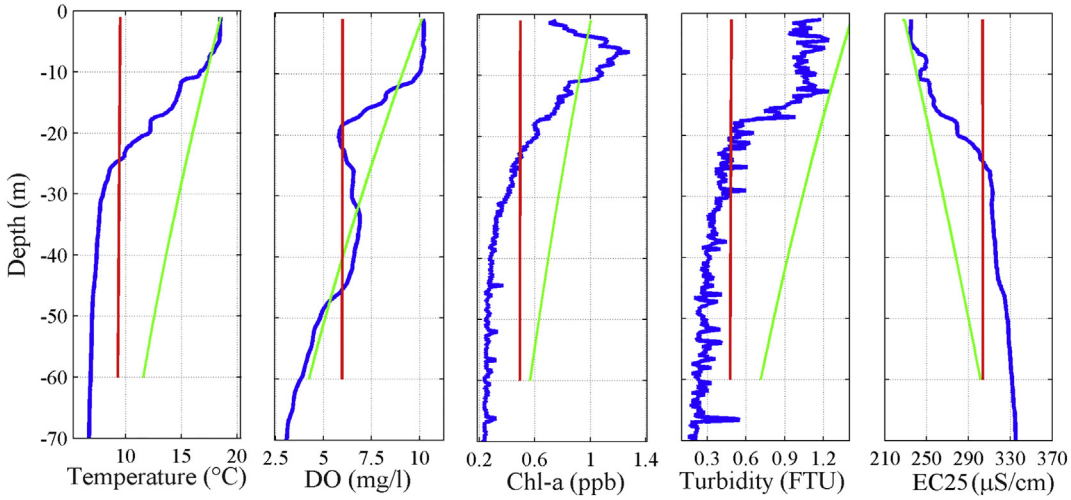

Fig. 12. Example of measured (blue solid line) and predicted profiles at point S3 in Fig. 1. The predicted profiles (IDW algorithm, red line, and Natural Neighbours method, green line) are computed only on the basis of the data measured at the surrounding sampling profiles and without the optimised vertical expansion of the data as applied in Fig. 5.

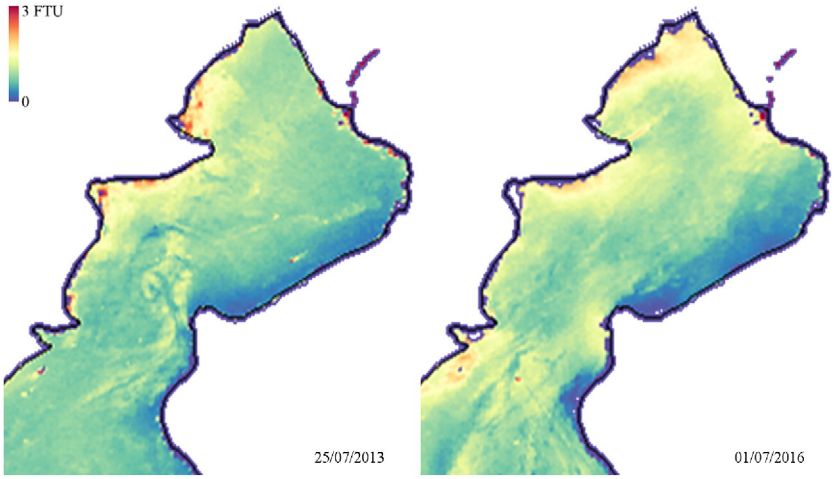

Fig. 13. Turbidity maps from Landsat-8 images obtained during thermally stratified periods (July 25, 2013 and July 1, 2016), when the average daily discharge was comparable to the ones of Fig. 10.

temperature at the thermocline would be almost equally affected by temperature at the surface, at the bottom and at the thermocline of surrounding measured vertical profiles.

In such an environment, an effective 3D interpolation scheme should introduce vertical anisotropy. The simplest way to do this is to segment data into layers, which is tantamount to repeatedly using a 2D interpolation approach that does not effectively utilize the measured information. This could be correct across the thermocline but could be questionable in the mixed epilimnion above and in the hypolimnion below. Another possibility is using different correlation coefficients along vertical and horizontal directions. Finally, a simple approach is the one introduced in this paper, that expands the distance of data in the vertical direction during the prediction phase, so fictitiously creating a lake whose horizontal direction is comparable to the vertical one.

One could expect that the layer thickness, the vertical correlation coefficient, and the expansion coefficient should all vary with depth. In such a case, the expansion coefficient should change its value along the vertical as a function of the local stability of the water column, being maximum close to the thermocline and smaller in the surface mixed layer and in the hypolimnion. To explore this, we have made some attempts to link α to the local value of the buoyancy frequency, but without obtaining a conclusive benefit with respect to the use of a simple constant coefficient. Here, the most likely problem is that the local buoyancy frequency is in itself a function of the unknown temperature profile.

The physical model provided a vehicle to isolate the role of the Coriolis' force on the plume of the two tributaries, that is usually not visible from the surface and is confounded with the combined effect of other dynamic forcings (e.g., wind and the seiche related flow field). Under ordinary flow conditions, the model predicts a systematic deflection of the tributary waters towards the western shore of the lake, triggering a clockwise gyre within the Lovere bay and a slow counterclockwise gyre that returns water towards the river mouth moving along the eastern shore. For higher flow rate discharges, the effect of the Earth's rotation weakens with respect to the plume's inertia in the entrance zone and it has a more rectilinear pattern. Accordingly, one could expect that the north-western part of the lake, although misaligned with respect to the tributaries axis, is systematically more sensitive to water quality degradation related to river-borne pollution. Suspended particles, containing nutrients and bacteria, could preferentially settle in this part of the lake, triggering metabolic processes that cause a general reduction of the oxygen concentration along the water columns. This will increase the fragility of this area with respect to eutrophication and algal blooms. Considering health risks associated with pollution of coastal bathing waters at the surface during the summer, the prevailing interflow mode, that usually occurs at a depth between 5 and 10 m, probably contributes to diminishing the risk for the north-western part of the lake but, on the basis of the obtained results, a more specific modeling effort (e.g., Antenucci et al., 2005) seems necessary.

In spite of the discussed simplifying assumptions, the area of influence of the tributaries deduced from the results of the physical model closely matches the one shown by the remote sensing image (see Figs. 9A and 11A). Both these tools are easy to understand and to communicate; thus, providing effective instruments to convey the concept of the lake's vulnerability to a lay audience. Actually there is a cross-fertilization process between these two results: the first explains the reason for the patterns shown by the second, that, in turn, provides an evident confirmation of the correctness of the physical model.

In this study, we found that a physical explanation of the observed processes resulted from the coupling of analysis of the remote sensing images with the other observations. The successful observation of the plume pattern in thermally unstratified periods would have been impossible during the prevailing thermally stratified period, whose extent is known thanks to the measurements of the lake and tributary temperatures. As shown in Fig. 13, the images obtained in the thermally stratified period do not indicate clear evidence of the westward drift but usually only a higher level of diffused turbidity on the western side of the lake. This is probably the result of the vertical mixing exerted by internal wave activity on the deeper tributary plumes. This underscores the importance of a stronger holistic approach coupling observations, experiments, and models in the investigation and understanding of remote sensing information.

Acknowledgments

This research is part of the ISEO (Improving the lake Status from Eutrophy to Oligotrophy) project and was made possible by a CARIPLO foundation grant number 2015-0241. The participation of SCC was supported by the Summer Visiting Professor Program at the Università degli Studi di Brescia. We are grateful to Ilaria Cazzaniga and Chiara Elli for supporting the satellite image processing. We are grateful to two anonymous Reviewers and to the Associate Editor for their contribution in the improvement of this paper.

References

Antenucci, J.P., Brookes, J.D., Hipsey, M.R., 2005. A simple model for quantifying cryptosporidium transport, dilution and potential risk in reservoirs. J. Am. Water Works Assoc. 97, 86–93.

Atkinson, J.F., Lin, G., Joshi, M., 1994. Physical model of Niagara River discharge. J. Great Lakes Res. 20, 583–589.
Bahner, L., 2006. User Guide for the Chesapeake Bay and Tidal Tributary Interpolator. NOAA Chesapeake Bay Office, Annapolis, Md.
Bonomi, G., Gerletti, M., 1967. Il Lago d'Iseo: primo quadro limnologico generale (termica, chimica, plancton e benton pro- fondo). Mem. Ist. Ital. Idrobiol. 22, 149–175.
Bouffard, D., Perga, M.E., 2016. Are flood-driven turbidity currents hot spots for priming effect in lakes? Biogeosciences 13 (3573–3584), 2016.
Brando, V.E., Braga, F., Zaggia, L., Giardino, C., Bresciani, M., Bellafiore, D., Ferrarin, C., Maicu, F., Benetazzo, A., Bonaldo, D., Falcieri, F.M., Coluccelli, A., Russo, A., Carniel, S., 2015. High resolution satellite turbidity and sea surface temperature observations of river plume interactions during a significant flood event. Ocean Sci. Discuss. 11, 909–920.
Chapra, S.C., 1997. Surface Water Quality Modeling. McGraw Hill.
Chen, X., Driscoll, C.T., 2009. Watershed land use controls on chemical inputs to Lake Ontario embayments. J. Environ. Qual. 38, 2084–2095.
Chen, C., Wang, L., Ji, R., Budd, J.W., Schwab, D.J., Beletsky, D., Fahnenstiel, G.L., Vanderploeg, H., Eadie, B.J., Cotner, J.B., 2004. Impacts of suspended sediment on the ecosystem in Lake Michigan: a comparison between the 1998 and 1999 plume event. J. Geophys. Res. 109, C10S05 (18 pp.).
Chipman, J.W., Lillesand, T.M., Schmaltz, J.E., Leale, J.E., Nordheim, M.J., 2004. Mapping lake water clarity with Landsat images in Wisconsin, U.S.A. Can. J. Remote. Sens. 30 (1):1–7. https://doi.org/10.5589/m03-047.
Chomicki, K.M., Howell, E.T., Defield, E., Dumas, A., Taylor, W.D., 2016. Factors influencing the phosphorus distribution near the mouth of the Grand River, Ontario, Lake Erie. J. Great Lakes Res. 42 (3), 549–564.
Dogliotti, A.I., Ruddick, K.G., Nechad, B., Doxaran, D., Knaeps, E., 2015. A single algorithm to retrieve turbidity from remotely-sensed data in all coastal and estuarine waters. Remote Sens. Environ. 530 (156):157–168. https://doi.org/10.1016/j.rse.2014.09.020.
European Parliament, 2000. Directive 2000/60/EC of the European Parliament and of the Council of 23 October 2000 Establishing a Framework for Community Action in the Field of Water Policy.
Fink, G., Wessels, M., Wüest, A., 2016. Flood frequency matters: why climate change degrades deep-water quality of peri-alpine lakes. J. Hydrol. (ISSN: 0022-1694) 540: 457–468. https://doi.org/10.1016/j.jhydrol.2016.06.023 (September 2016).
Foley, J.D., van Dam, A., Hughes, J.F., Feiner, S.K., 1990. Spatial-partitioning representations; surface detail. Computer Graphics: Principles and Practice. The Systems Programming Series. Addison-Wesley, Boston. ISBN: 0-201-12110-7.
Griffiths, R.W., 1986. Gravity currents in rotating systems. Annu. Rev. Fluid Mech. 18, 59–89.
Hakanson, L., 1974. Mercury in some Swedish lake sediments. Ambio 3, 37–43.
Hakanson, L., Janson, M., 1983. Principles of Lake Sedimentology. Springer, Berlin, Germany.
Halder, J., Decrouy, L., Vennemann, T.W., 2013. Mixing of Rhône River water in Lake Geneva (Switzerland–France) inferred from stable hydrogen and oxygen isotope profiles. J. Hydrol. (ISSN: 0022-1694) 477:152–164. https://doi.org/10.1016/j.jhydrol.2012.11.026 (16 January 2013).
Hamblin, R.E., Carmack, E.C., 1978. River-induced currents in a fjord lake. J. Geophys. Res. 63, 885–899.
Hogg, C.A.R., Marti, C.L., Huppert, H.E., Imberger, J., 2013. Mixing of an interflow into the ambient water of Lake Iseo. Limnol. Oceanogr. 58 (2):579–592. https://doi.org/10.4319/lo.2013.58.2.0579.
Kreling, J., Bravidor, J., Engelhardt, C., Hupfer, M., Koschorreck, M., Lorke, A., 2016. The importance of physical transport and oxygen consumption for the development of a metalimnetic oxygen minimum in a lake. Limnol. Oceanogr. https://doi.org/10.1002/lno.10430.
Laborde, S., Antenucci, J.P., Copetti, D., Imberger, J., 2010. Inflow intrusions at multiple scales in a large temperate lake. Limnol. Oceanogr. 55, 1301–1312.
Lathrop Jr., R.G., Vande Castle, J.R., Lillesand, T.M., 1990. Monitoring river plume transport and mesoscale circulation in Green Bay Lake Michigan USA through satellite remote sensing. J. Great Lakes Res. 16 (3), 471–484.
Li, J., Heap, A.D., 2011. A review of comparative studies of spatial interpolation methods in environmental sciences: performance and impact factors. Ecol. Inform. 6 (2011), 228–241.
Li, C., Kisser, K.M., Rumer, R.R., 1975. Physical model study of circulation patterns in Lake Ontario. Limnol. Oceanogr. 203, 323–337.
Li, C., Walker, N., Hou, A., Georgiou, I., Roberts, H., Laws, E., McCorquodale, J.A., Weeks, E., Li, X., Crochet, J., 2008. Circular plumes in Lake Pontchartrain estuary under wind straining. Estuarine Coast. Shelf Sci. (ISSN: 0272-7714) 80 (1):161–172. https://doi.org/10.1016/j.ecss.2008.07.020.
Li, W., Liu, W.L., Zhang, Y., Yin, W., Liu, Y., 2010. On the comparison of spatial interpolation methods of marine temperature and salinity based on ARGIS software: a case study of Tianjin coastal waters in the Bohai Bay. In: Guo, H., Wang, C. (Eds.), Sixth International Symposium on Digital Earth: Models, Algorithms, and Virtual Reality, Beijing, People's Republic of China. SPIE Press, Bellingham, WA.
Li, J., Heap, A.D., Potter, A., Daniell, J.J., 2011. Application of machine learning methods to spatial interpolation of environmental variables. Environ. Model Softw. 12 (26), 1647–1659.
Morillo, S., Imberger, J., Antenucci, J.P., Woods, P.F., 2008. The influence of wind and Lake Morphometry on the interaction between two rivers entering a stratified lake. J. Hydraul. Eng. 134, 1579–1589.
Mortimer, C.H., 2006. Inertial oscillations and related internal beat pulsations and surges in Lakes Michigan and Ontario. Limnol. Oceanogr. 51 (5), 1941–1955.
Murphy, R., Curriero, F., Ball, W., 2010. Comparison of spatial interpolation methods for water quality evaluation in the Chesapeake Bay. J. Environ. Eng.:160–171 https://doi.org/10.1061/(ASCE)EE.1943-7870.0000121.
Özkundakci, D., Hamilton, D.P., Kelly, D., Schallenberg, M., De Winton, M., Verburg, P., Trolle, D., 2014. Ecological integrity of deep lakes in New Zealand across anthropogenic pressure gradients. Ecol. Indic. 37, 45–57.
Pahlevan, N., Lee, Z., Wei, J., Schaaf, C.B., Schott, J.R., Berk, A., 2014. On-orbit radiometric characterization of OLI (Landsat-8) for applications in aquatic remote sensing. Remote Sens. Environ. 154:272–284. https://doi.org/10.1016/j.rse.2014.08.001.
Pilotti, M., Valerio, G., Leoni, B., 2013. Data set for hydrodynamic lake model calibration: a deep pre-Alpine case. Water Resour. Res. 49:7159–7163. https://doi.org/10.1002/wrcr.20506.
Pilotti, M., Valerio, G., Gregorini, L., Milanesi, L., Hogg, C., 2014a. Study of tributary inflows in Lake Iseo with a rotating physical model. J. Limnol. 73 (1). https://doi.org/10.4081/jlimnol.2014.772.
Pilotti, M., Simoncelli, S., Valerio, G., 2014b. A simple approach to the evaluation of the actual water renewal time of natural stratified lakes. Water Resour. Res. 50 (4): 2830–2849. https://doi.org/10.1002/2013WR014471.
Rumer, R.R., Robson, L., 1968. Circulation Studies in a Rotating Model of Lake Erie. State University of New York at Buffalo (36 pp.).
Sahlin, J., Mostafavi, M.A., Forest, A., Babin, M., 2014. Assessment of 3D spatial interpolation methods for study of the marine pelagic environment. Mar. Geod. 37 (2): 238–266. https://doi.org/10.1080/01490419.2014.
Stewart, K.M., 1988. Tracing inflows in a physical model of Lake Constance. J. Great Lakes Res. 14 (466), 478.
Strömbeck, N., Pierson, E., 2001. The effects of variability in the inherent optical properties on estimations of chlorophyll a by remote sensing in Swedish freshwater. Sci. Total Environ. 268, 123–137.
Toming, K., Kutser, T., Laas, A., Sepp, M., Paavel, B., Nõges, T., 2016. First experiences in mapping lake water quality parameters with sentinel-2 MSI imagery. Remote Sens. 8 (8), 640.
USEPA, Region III Water Protection Division, 2007. Ambient water quality criteria for dissolved oxygen, water clarity and chloro-phyll a for the Chesapeake Bay and its tidal tributaries 2007 addendum. Rep. No. EPA 903-R-07-003, U.S. Environmental Protection Agency Region III, Chesapeake Bay Program Office, and Region III Water Protection Division, Annapolis, Md.
Valerio, G., Pilotti, M., Marti, C.L., Imberger, J., 2012. The structure of basin scale internal waves in a stratified lake in response to lake bathymetry and wind spatial and temporal distribution: Lake Iseo, Italy, Limnol. Oceanography 57 (3), 772–786.
Vanhellemont, Q., Ruddick, K., 2014. Turbid wakes associated with offshore wind turbines observed with Landsat 8. Remote Sens. Environ. 145:105–115. https://doi.org/10.1016/j.rse.2014.01.009.
Vanhellemont, Q., Ruddick, K., 2015. Advantages of high quality SWIR bands for ocean colour processing: examples from Landsat-8. Remote Sens. Environ. 161:89–106. https://doi.org/10.1016/j.rse.2015.02.007.
Wetzel, R.G., 1992. Clean water: a fading resource. Hydrobiologia 243, 21–30.
Wetzel, R.G., 2001. Limnology. 3rd ed. Academic Press.
Wright, R.F., Nydegger, P., 1980. Sedimentation of detrital particulate matter in lakes: influence of currents produced by inflowing rivers. Water Resour. Res. 16, 597–601.
Zhang, Y., Shi, K., Zhou, Y., Liu, X., Qin, B., 2016. Monitoring the river plume induced by heavy rainfall events in large, shallow, Lake Taihu using MODIS 250 m imagery. Remote Sens. Environ. 173, 109–121.
Zimmerman, D., Pavlik, C., Ruggles, A., Armstrong, M.P., 1999. An experimental comparison of ordinary and universal kriging and inverse distance weighting. Math. Geol. 31 (4), 375–390.